



Numerical Analysis of the Turbulent Flow Structure Induced by the Cavitation Shedding using LES

H. Kanfoudi[†], G. Bellakhall, M. Ennouri, A. Bel Hadj Taher and R. Zgolli

Laboratory of Hydraulic and Environmental Modeling, National Engineering School of Tunis, University of Tunis EL MANAR, 1002 Tunis, Tunisia.

[†]Corresponding Author Email: hatem.kanfoudi@enit.rnu.tn

(Received November 11, 2016; accepted February 6, 2017)

ABSTRACT

To analyze the interaction between the turbulent flow structure with the cavitation shedding dynamics, a three-dimensional unsteady cavitating turbulent flow around the three-dimension NACA009 hydrofoil is investigated in this study. The cavitating flow in has been modeled with a homogeneous mixture of liquid and vapor using LES. The interaction between the cavitation and the fluid vortex is analyzed and discussed. The results demonstrate that the vortex stretching is mainly in the center of the cloud cavity and changes quasi-periodically as the cloud cavity evolves. As a result, the mechanism of the inception of cavitation, re-entrant jet and cavitation cloud shedding are accurately captured and predicted by LES in accordance with the experiment data.

Keywords: NACA0009 hydrofoil; Sheet/cloud cavitation; LES; Cavitation; Vortex interaction; Unsteady flow; Fluid structure; Pressure fluctuations.

NOMENCLATURE

C_D	drag coefficient	R_0	initial radius of bubble
C_L	lift coefficient	Re	Reynolds number
C_μ	dimensionless constants	Str	Strouhal number
$Drag$	drag force	U_∞	inlet flow velocity
Lift	lift force	V_{vap}	volume of vapor in control cell
\dot{m}	source term	V_{vap}	vapor volume
\dot{m}^+	vaporization source term	y^+	normal dimensionless distance to the wall
\dot{m}^-	condensation source term	α_v	vapor volume fraction
n_0	nuclei concentration per unit volume of pure liquid	μ	vapor viscosity
P_∞	outlet pressure	μ_v	liquid viscosity
P_v	vapor pressure	μ_t	eddy viscosity
R	bubble radius	ρ_l	liquid density
		ρ_v	vapor viscosity

1. INTRODUCTION

Cavitation pocket formed around the hydrofoil could produce pressure fluctuations when collapsing in the high-pressure region at the trailing edge causing material erosion. The interest in the leading edge cavitation is motivated by two reasons; first this is the main cavitation type encountered in hydraulic machinery and is at the origin of the head drop phenomenon, and second, the leading edge cavitation is known as the most erosive one,

because of its attachment to the blade and near-wall induced bubbles collapse. Due to this complex behavior, many authors have conducted many research for understand this mechanism(Goncalves, Decaix, and Patella 2010; Kuijpers *et al.* 2002; Martynov 2005; Salleo *et al.* 2000; Schnerr, Sezal, and Schmidt 2008; Wang and Su 2010). The complexity of the phenomenon make cavitation modelling difficult in the sense that experimental investigations require specific instrumentation for

the multiphase environment, and the modelling strategies have to be based on empirical hypothesis. Nevertheless the researchers have made great efforts, starting from the work of (Rayleigh 1917) up to today, a lot of theoretical and experimental research has been conducted in order to analyze and understand the cavitation phenomenon. In experimental studies, an extensive amount of literature exists, dealing with different aspects of cavitation. Most of them are dedicated to fundamentals aspect, and the physics of cavitation. Numerical studies and simulations of cavitation have been pursued for years, even if the Navier-Stokes based simulations emerged only in the last decade. Existing cavitation models compute the overall behavior of cavitating flows which implies that the major goal of a cavitation model should be to predict the onset, growth, and collapse of bubbles in cavitating flows. There is no comprehensive model in the literature that can simulate various types of cavitation and provide a detailed description of the flow field.

Many experiments have been conducted to identify the precise mechanisms responsible for the complex features of cavitating flows (Chen, G.H., Wang, G.Y., Huang, B., Hu, C.L., Wang, Z.Y., Wang 2015)(Ji *et al.* 2014)(Zhao, Wang, and Huang 2016a). Depending on the operating conditions many types of cavitation can be observed on a cavitating hydrofoil: bubble, sheet, cloud and vortex cavitation. (Wang *et al.* 2001) According to (Arndt 1981), the main two parameters responsible of the cavitation inception are the density of bubble contained in the fluid and nuclei size.

A more detailed study realized by (Katz, J., O'Hern 1986) shows that the cavitation inception was found to occur in the axial vortices mainly in the portion between the spanwise eddies. At lower pressures cavitation takes the form of the spanwise vortices but the axial vortices always remain evident. A recent experiment performed by (Kravtsova, A.Y.; Markovich, D.M.; Pervunin, K.S.; Timoshevskiy and Hanjalić 2014) around a NACA0015 hydrofoil showed that the incipience of cavitation is governed by the development of the carrier-fluid flow around the foil leading edges.

Many of published research focused on the jet returning mechanism since it is responsible of the cloud cavity shedding (Altimira, M.; Fuchs 2015); (Arndt 2001);(Dreyer, M.; Decaix, J.; Münch-Alligné, C.; Farhat 2014); (Goncalvès, E.; Charrière 2014);(Roohi, E.; Zahir, A.P.; Passandideh-Fard 2013); (Yu, X., Huang, C., Du, T.; Liao, L.; Wu, X.; Zheng, Z.; Wang 2014) (Huang, Wang, and Zhao 2014). Referring to the results of the measurement of the re-entrant jet thickness performed by (Callenaere *et al.* 2001), they concluded that the dynamic behaviour of a partial cavity depending of the pressure gradient. When the adverse pressure gradient at cavity closure is high enough, a re-entrant jet will develop at the back of the cavity. Also, they mentioned for thick enough cavities, the re-entrant jet does not interact significantly with the cavity interface as it moves upstream.

(Foeth *et al.* 2006) carried out experiments for the 3D Twist11 hydrofoil in steady and unsteady inflow conditions in the cavitation tunnel at Delft University. Their focus was to generate sheet cavities that are three-dimensional in character similar to ones that occur on ship propellers. Based on experimental observation (Ji *et al.* 2014). They demonstrate that the shedding is periodic, constant in its shedding frequency, and always includes the same macro structural collapse (Foeth *et al.* 2006).

Further study using three dimensional simulations are needed to validate the hypothesis of the connection between the entrainment ability and the re-entrant jet. In parallel, experimental techniques are significantly to better, for understand the mechanism and this link.

(Wosnik, M., Arndt, R., Ain 2006) documented the unsteady cavitation shedding, to study the complex flow characteristics around two-dimensional NACA0015 hydrofoil. They concluded that time-resolved PIV holds the promise of providing us with whole-field, high-resolution, timeresolved, quantitative experimental data of cavitating flows. This wealth of information can typically only be obtained from DNS or LES.

In some experimental measurement techniques, some devices do not access to the measurements, which leads to development of the numerical tools in recent years. Computational methods for cavitating flows have evolved in parallel with computational resources. In spite of the improved experimental techniques, numerical simulations are attracting more and more interest with noticeable success in predicting cavitating flows in recent years (Luo, X.-w.; Ji 2016)(Pendar, M.-R.; Roohi 2016)(Peng, X.X.; Ji, B.; Cao, Y.; Xu, L.; Zhang, G.; Luo, X.; Long 2016)(Timoshevskiy, M.V.; Churkin, S.A.; Kravtsova, A.Y.; Pervunin, K.S.; Markovich, D.M.; Hanjalić 2016)(Wu, X.C., Wang, Y.W., Huang 2016)(Zhu *et al.* 2015)

For simulation the cavitation flow, many approach has been developed during the recent years. Based on (ITTC 1999) , four technique has been employed, Interface-tracking methods ((Hutton, R.A.;Furness 1975), (Chen, Y.; Heister 1994) , (Deshpande, M.; Feng, J.; Merkle 1998), (Hirschi, R.; Dupont, Ph.; Avellan, F.; Favre, J.N.; Guelich, J.F.; Parkinson 1998), Volume-of-Fluid methods ((Dieval, L.; Arnoud 1998), (Molin, B.; Dieval, L. , Marcer 1997) and. (Sauer, J.; Schnerr 2000) developed a VoF method with bubble dynamics based on the Rayleigh equation, see also(Yuan, W.;Sauer, J.; Schnerr 2001).), Discrete-bubble methods (Fujikawa, S.;Akamatsu 1980) and Two-phase flow methods (Kubota, A.; Kato 1992)(Sauer, J.; Schnerr 2000; Yuan, W.;Sauer, J.; Schnerr 2001) (Koop 2008; Kozubková, Rautová, and Bojko 2012), (Zwart, P.J.;Gerber, A.G.; Belamri 2004) and (Kanfoudi 2011, 2012, 2014, 2015)

For Two-phase flow methods, many proposed numericals models have been developed. This technique can be generally divided into two main types based on the method to determine the mixture

density as the Barotropic equation models (BEM) and the Transport equation based models (TEM). (Senocak and Shyy 2004) demonstrate that the BEM is not able to modeling the cavitating flow, and suggesting that the TEM can accommodate the baroclinic vorticity generation.

TEM eliminates the problem of baroclinic torque. Many sources terms of TEM are proposed in literature (Kanfoudi 2011) (Singhal *et al.* 2002) (Zwart, P.J.;Gerber, A.G.; Belamri 2004) (Kunz *et al.* 2003)(Yuan, Sauer, and Schnerr 2001). Owing to their success in capturing the features of cavitation flows, the (Kanfoudi 2011) cavitation model is used in the present paper.

Due to unsteady nature of the cavitating flow and the strong interaction within the flow and the boundary layer, it is imperative to model the cavitation flow using LES.

In cavitating flows, instabilities and turbulence often result in the formation of large-scale vortical structures. The unsteady cavitating flow is usually turbulent flow, it occurs for a high Reynolds number, to capture the mechanism of re-entrant jet for simulation the periodic shedding of the cavitation pocket, we need to modelling the turbulence model because it can significantly influence the cavitating flow structure. Recently revealed by researchers (Wu, Wang, and Shyy 2005), a serious repercussion of the modeling of turbulence on the simulation the unsteady cavitating flow.

To reproduce faithfully numerically the detachment mechanism of cavitation pocket, the Direct Numerical Simulations (DNS) are certainly the most accurate, but it requires a lot of extreme demand for computational resources. Originally proposed by (Smagorinsky 1963) and refined by many researchers, the large eddy simulation (LES) approach give better predictions of larger-scale turbulent eddies for modeling the cavitating flow. (Dittakavi, Chunekar, and Frankel 2010);(Yu, X., Huang; C., Du, T.; Liao, L.; Wu, X.; Zheng, Z.; Wang 2014); (Ji *et al.* 2014);(Ji *et al.* 2013, 2014);(Roohi, Zahiri, and Passandideh-Fard 2013);(Wang *et al.* 2005);(Amromin *et al.* 2006);(Zhao, Wang, and Huang 2016b).

The present study investigates cavitating flows around a three-dimension NACA0009 hydrofoil using the (Kanfoudi 2011) (Kanfoudi 2015) cavitation model coupling with LES. The interactions between the cavitation and the vortex formation. The evolution of the entrainment ability is investigated in a three-dimensional to analyze the mechanism of re-entrant jet and the processes of the cavitating shedding . The main objective of the present paper is to investigate the effect of cavity growth and shedding on the dynamics of vortical flows in unsteady flows over a NACA0009 hydrofoil. This paper, we will simulate the dynamics of a developed cavitation pocket.

The global validation of the numerical simulation is based on the experimental results of Power Spectral Density (PSD) (AitBouziad 2005).

2. MATHEMATICAL FORMULATIONS

2.1 Governing Equations

In the mixture model for vapor/liquid two-phase flows, the multiphase fluid components are assumed to share the same velocity and pressure.

The continuity and momentum equations for the mixture flow equations are,

$$\frac{\partial \rho_m}{\partial t} + \frac{\partial (\rho_m u_j)}{\partial x_j} = 0, \quad (1)$$

$$\frac{\partial (\rho_m u_i)}{\partial t} + \frac{\partial (\rho_m u_i u_j)}{\partial x_j} = \frac{\partial P}{\partial x_j} + \frac{\partial}{\partial x_j} \left(\mu \frac{\partial u_i}{\partial x_j} \right) \quad (2)$$

where u_i the velocity in x direction and P is the pressure. Laminar viscosity μ and density ρ_m are defined viscosity, respectively :

where :

$$\begin{aligned} \mu &= \alpha_v \mu_\alpha + (1 - \alpha_v) \mu_l \\ \rho_m &= \alpha_v \rho_\alpha + (1 - \alpha_v) \rho_l \end{aligned} \quad (3)$$

Applying a filtering operation to Eqs. (1) and (2) gives the LES equations:

$$\frac{\partial \rho_m}{\partial t} + \frac{\partial (\rho_m \bar{u}_j)}{\partial x_j} = 0 \quad (4)$$

$$\begin{aligned} \frac{\partial (\rho_m \bar{u}_i)}{\partial t} + \frac{\partial (\rho_m \bar{u}_i \bar{u}_j)}{\partial x_j} &= \frac{\partial \bar{p}}{\partial x_j} \\ + \frac{\partial}{\partial x_j} \left(\mu \frac{\partial \bar{u}_i}{\partial x_j} \right) - \frac{\partial \bar{\tau}_{ij}}{\partial x_j} \end{aligned} \quad (5)$$

where the over bars denote filtered quantities.

The Sub-grid Scale (SGS) stresses :

$$\tau_{ij} = \rho_m (u_i u_j - \bar{u}_i \bar{u}_j) \quad (6)$$

One commonly used SGS model is the eddy-viscosity model, which assumes that the SGS stresses are proportional to the modulus of the strain rate tensor, \bar{S}_{ij} , of the filtered large-scale flow:

$$\tau_{ij} - \frac{1}{3} \tau_{kk} \delta_{ij} = -2 \mu_t \bar{S}_{ij} \quad (7)$$

where \bar{S}_{ij} is the rate-of-strain tensor for the resolved scale and the sub-grid scale turbulent viscosity, μ_t , is closed by the LES Wall-Adapting Local Eddy-Viscosity (WALE) model (Koo *et al.* 2013).

2.2 Physical cavitation Model

The cavitation process is governed by the following

mass transfer equation,

$$\frac{\partial(\rho_v \alpha_v)}{\partial t} + \frac{\partial(\rho_v \alpha_v u_i)}{\partial x_i} = m^+ - m^- \quad (8)$$

where α_v is the vapor volume fraction, m^+ and m^- are the mass transfer rate for the vaporization and condensation processes, respectively. They are defined as :

$$m^+ = C_e \alpha_v^{\frac{2}{3}} (1 - \alpha_v)^{\frac{4}{3}} \frac{\rho_v \rho_l}{\rho_m} \sqrt{\frac{2}{3} \frac{p_v - p}{\rho_l}} \quad (9)$$

$$m^- = C_c \alpha_v^{\frac{1}{6}} (1 - \alpha_v)^2 \frac{\rho_v \rho_l}{\rho_m} \sqrt{\frac{2}{3} \frac{p - p_v}{\rho_l}}$$

with :

$$C_c = -10 R_0^{\frac{3}{2}} n_0^{\frac{5}{6}} \quad (10)$$

$$C_e = 5 \sqrt[3]{n_0} \quad (11)$$

where R_0 is the initial bubble radius, n_0 is defined as nuclei concentration per unit volume of pure liquid. This two parameter are related by the expression of the vapor volume fraction (Yuan *et al.* 2001; Yuan, W.; Sauer, J.; Schnerr 2001).

$$\alpha_v = \frac{n_0 \frac{4}{3} \pi R^3}{1 + n_0 \frac{4}{3} \pi R^3} \quad (12)$$

the value of nuclei concentration $n_0 = 510^{14}$ nuclei/m³ and the initial bubble radius $R_0 = 5 \mu m$ (Kanfoudi 2011).

This cavitation model, which is based on the modified model of Rayleigh Plesset, has been validated in many cases, such as cavitating flow around a 2D hydrofoil (Kanfoudi 2012; Kanfoudi 2011; Kanfoudi 2015) and 3D hydrofoil (Kanfoudi 2014).

3. SIMULATION SETUP

For numerical simulations, we used the Ansys CFX CFD code, with an incompressible solver.

A three dimensions' numerical simulation has been achieved for the study the unsteady cavitation flow around NACA0009. As an initial condition, we use a steady cavitating flow field to accelerate the computation of the cavitation pocket.

The hydrofoil chord was $c = 110$ mm with a relative maximum thickness of 9% at 50% chord length from the leading edge. The hydrofoil is inclined by 5° relative to the direction of flow as shown in Fig. 1.

As boundary condition, the inflow velocity was $U_\infty = 20$ m/s and for the outflow, a static pressure calculated according the cavitation number:

$$\sigma = (p_{out} - p_v) / \left(\frac{1}{2} \rho_l U_\infty^2 \right) \quad (13)$$

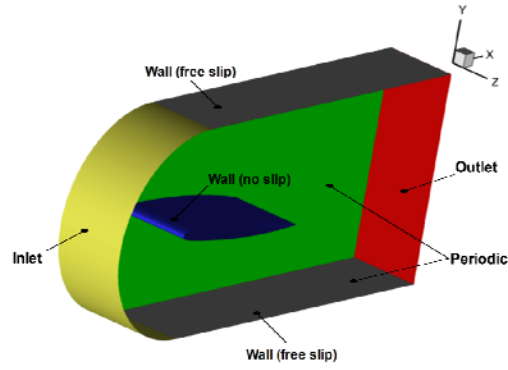


Fig. 1. Computation domain.

The Reynolds number can be express by:

$Re = \rho_l U_\infty c / \mu_l$, in this simulation the number of Reynolds is $2 \cdot 10^6$. Thus, the flow regime is turbulent.

For the calculation procedure, a time step was set to 10^{-5} s dependent to CFL number. The convergence criteria used the RMS residual type with a residual target of 10^{-5} , for more accuracy of the numerical results.

Numerically, it is very difficult to use the real spanwise size of the NACA0009 hydrofoil, this is due to computation resource. That is why, the spanwise size adopted in this study is 0.5 chord, this choice is justified by (Sagaut 2005). They justified their publication, that for spanwise twice the thickness of the hydrofoil, it is sufficient to resolve streamwise vortex.

The Fig. 2 shows the computational domain and boundary conditions. The lateral boundary condition, were set respectively, one as non-slip, the other as periodic condition.

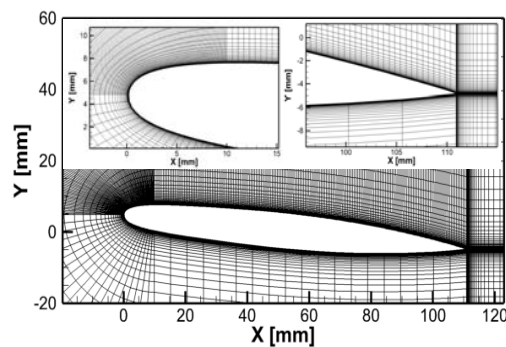


Fig. 2. Mesh spacing around NACA0009 hydrofoil.

Because of the numerical solution is influenced by the mesh topologies, a 3-D structured mesh C-grid type is applied in this investigation to study the unsteady cavitation flow, this type of mesh is best choice for mesh around the hydrofoil. For this reason, we can concentrate directly a high number of nodes to capture the boundary layer, the pressure gradient and the flow separation at the trailing edge.

To modeling accurate, the boundary layer on the hydrofoil, we used Automatic Near-Wall Treatment. This technique can resolve the viscous sublayer (Wilcox 1988; Wilcox 1994),(Menter 1994).To capture numerically the boundary layer a value of $y^+ = 1$ is used, the Fig.2 show the spacing of the grid around the hydrofoil.

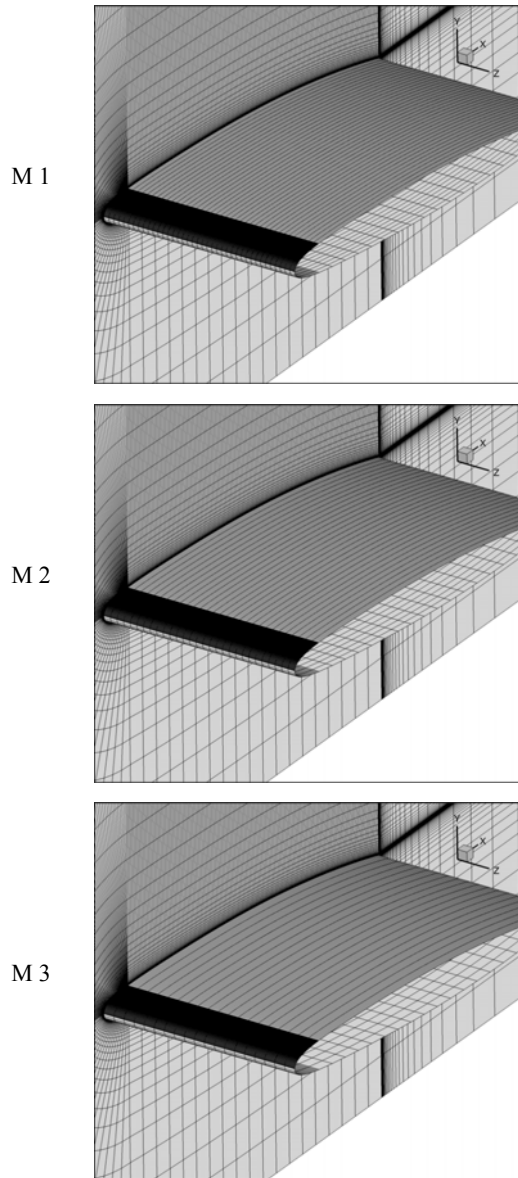


Fig. 3. The three tested structured grid.

The numerical solution is sensitive to the mesh resolution. In order to ensure the dependence of the numerical solution of the number of nodes, we conducted numerical simulation of three grids, the criteria of choice are the coefficient of lift and drag values in stationary flow regime. The expressions of the coefficient of lift and drag are illustrated as follows:

$$C_L = \frac{Lift}{\frac{1}{2} \rho_l U_\infty^2 c_{spanwise}}$$

$$C_D = \frac{Drag}{\frac{1}{2} \rho_l U_\infty^2 c_{spanwise}} \quad (14)$$

The Fig. 3 present, the three meshes quality around the NACA0009 hydrofoil. The Table 1 shows the variations of the coefficient of lift and drag as a function of the nodes number

In order to reduce the numerical diffusion for the pressure calculation at the leading edge of the hydrofoil, we refine the mesh in this region.

As results from this three mesh, there is no difference between the medium and the fine meshes. Thus, the middle resolution mesh was chosen for simulation the unsteady the cavitating flow.

Table 1 Mesh independence test

Mesh resolution	Cells	C_L	C_D	
M 1	fine	792000	0.20177	0.0324
M 2	medium	588294	0.20170	0.0322
M 3	coarse	385000	0.19210	0.0298

For the computing resources, the unsteady computations are done using Dell PowerEdge 720 with 16 processors (4 sockets and 4 cores) Intel® Xeon® E5-2600 2.2 GHz and 64 Go Ram memory.

The CPU time is 20 h for each process of cavitating shedding.

4. RESULTS AND DISCUSSION

The numerical simulation in this paper, aim to analyze and study the dynamic mechanism of the sheet cavitation shedding using LES. The validation of this numerical model is performed with the experimental data available from (AitBouziad 2005).

To better detect the evolution of detachment of the shedding cavity, we use numerically V_{vap} which is a practical parameter for the unsteady cavitating flow simulation, his expression is given as follows:

$$V_{vap} = \frac{1}{c^3} \sum_{i=1}^N \alpha_i V_i \quad (15)$$

where N denote the number of the control volumes, α_i the vapor volume fraction occupied and the total volume of each control volume in the computational domain.

For practical reasons, all results are presented as dimensionless numbers in the following discussion.

Fig.4-a shows the variation of the total vapor volume in twelve typical periods. To identify

the process of cavitating shedding, we present in Fig 4-b one cycle of formation and destruction of the vapor pocket on the extrados of NACA0009 hydrofoil.

To study the dynamics of detachment of the cavitation pocket and its effect on the flow, we will be limited to 10 typical instants as shown in Figure 4-b.

In fig. 4 the cyclic behavior of the vapor sheet and its shedding are presented at ten equidistant time-instants. The period T^* of the cycle is $T^* = 0.008$ s and $f_{cycle} = 122$ Hz with $Stc = 0.61$.

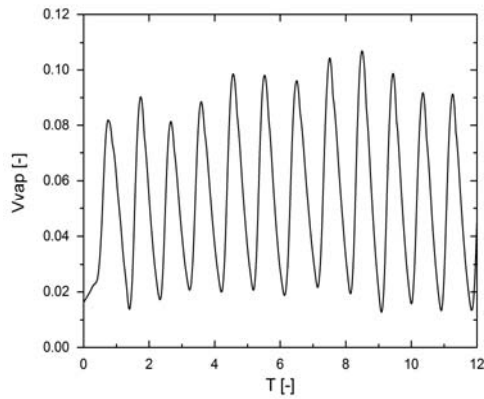


Fig. 4-a. Total vapor volume computed.

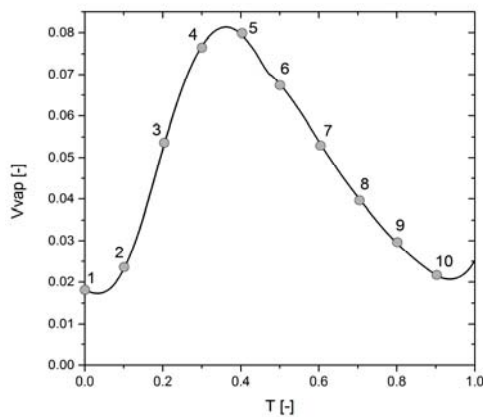


Fig. 4-b. Vapor volume for one cycle.

The power spectrum density (PSD) of the velocity on direction x for $x/c=0.3$ for twelve periods of the cavitation shedding is shown in Fig. 5.

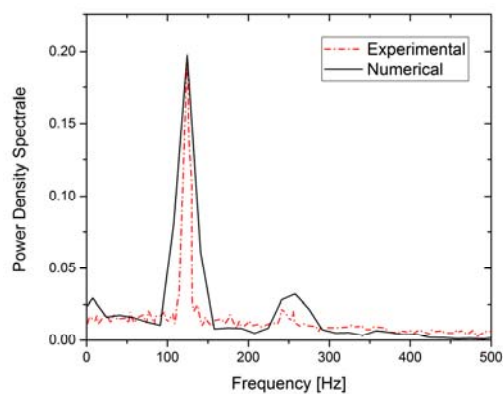


Fig. 5. Comparison of the unsteady cavitation amplitude spectrum.

It is clear that the frequency of detachment of the cavitation cavity is $f = 122$. The transitory nature of the evolution of the vapor cavity acts directly on the flow structures. Both, the fluctuation of the velocity on the suction surface of the hydrofoil and the vapor volume has the same frequency.

By comparing experimental data of PDS with the numerical results in Fig. 5, we can note that the numerical model can predict and reproduce in 3D the evolution of the cavitation pocket. We can presume that the overall evolution of the cavity volume agrees well with the experimental data.

It is clear, that the present numerical model is in agreement with the experimental data for the cavitation shedding dynamics.

By plotting the PSD of the velocity in Fig.6, the plot exhibit power law behavior of the energy spectrum with a slope equal to $-5/3$. This value was determined by Kolmogorov theory which introduced the concept of universality of locally homogenous and isotropic turbulence for fully developed turbulence at high Reynolds numbers (Shia-Hui and ;Werner 2008; Walters *et al.* 2013; Shur *et al.* 2008; Davidson & Peng 2003) (Pope 2000).

This result is important; it demonstrates that the turbulence model employed in this study is able to capture the turbulence spectrum like LES. For a low frequency, there is a production of kinetic energy from the large structures flow and then this energy is transferred and finally for a high frequency we assist to the destruction and dissipation of this energy into a small structure which is the source of production of the re-entrant jet for the cavitating shedding.

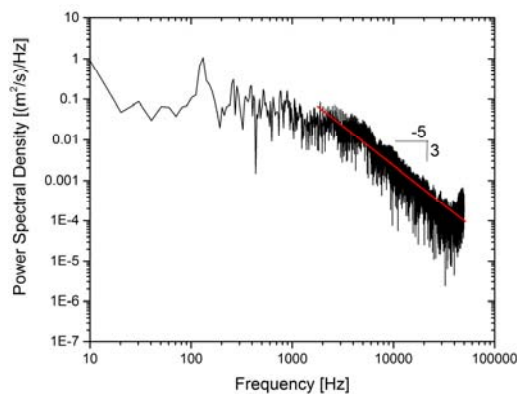


Fig. 6. Power spectrum density of velocity at $x/c=0.3$.

Fig.7 shows the time evolution of the calculated cavitation shedding for ten snapshots of the typical instants in a cycle. During this process, 7-2 to 7-5, the cavity growth continues and the behavior of the cavity seems to be stable. The length of the cavity reaches the half of the chord and she becomes thicker. At 7-6, at the middle of spanwise of the hydrofoil, the re-entrant jet appears and produces a noticeable effect on the cavity shape. The re-entrant jet continuous moves to the leading edge and

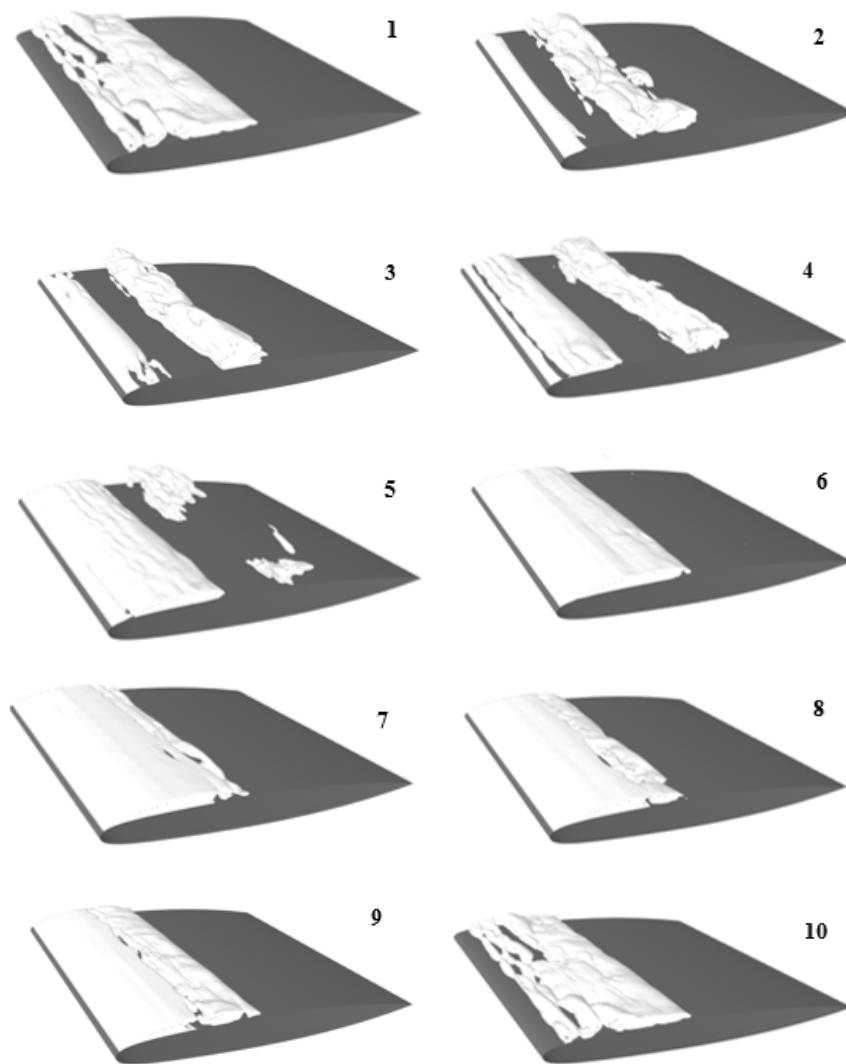


Fig. 7. Time evolution of the cavitation shedding.

destroy the interface between the vapor and the hydrofoil wall (Fig. 7-7 to 7-9), after the development of the re-entrant jets at the closure region, the main sheet vapor is split into a small sheet vapor. The shed cavitation cloud is advected downstream with the main flow and finally collapses. (Fig. 7-10 and Fig.7-1). The leading edge of the hydrofoil is now free of vapor and a new vapor sheet starts to grow. This process is repeated continuously.

For describe the mechanism of the cavitation shedding, we present in Fig. 8 the pressure gradient distribution on the x direction and the cavity shape for one cycle.

At time 1, a negative pressure gradient is located at the nose of the hydrofoil which cause a depression in the extrados of this one, allowing the sheet cavity to starting to grow at the leading edge of the hydrofoil. The shed vapor cavity, extracted from the previous cycle, is convected at the middle of the

hydrofoil, we can highlight the dominance of the negative pressure gradient at the front of the shed vapor cavity compared to the positive pressure gradient, hence we can justify the displacement and the rotation of this one to the trailing edge.

From time 2 to 4, the shed vapor cavity collapses at the trailing edge of hydrofoil, this is due to the liquid pressure. The sheet cavity continues to grow and reached its maximum length and she becomes thicker.

As the pocket cavitation becomes thick, it will cause a flow separation in the closure region of the main cavity. This is noticeable in the pressure gradient, a positive pressure gradient at the end of the pocket will favor the development of re-entrant flow (at time 5 and 6). We note also the small vortical flow at the closure region of the cavity.

The high positive pressure gradient leads to the formation of the re-entrant jet, which travels

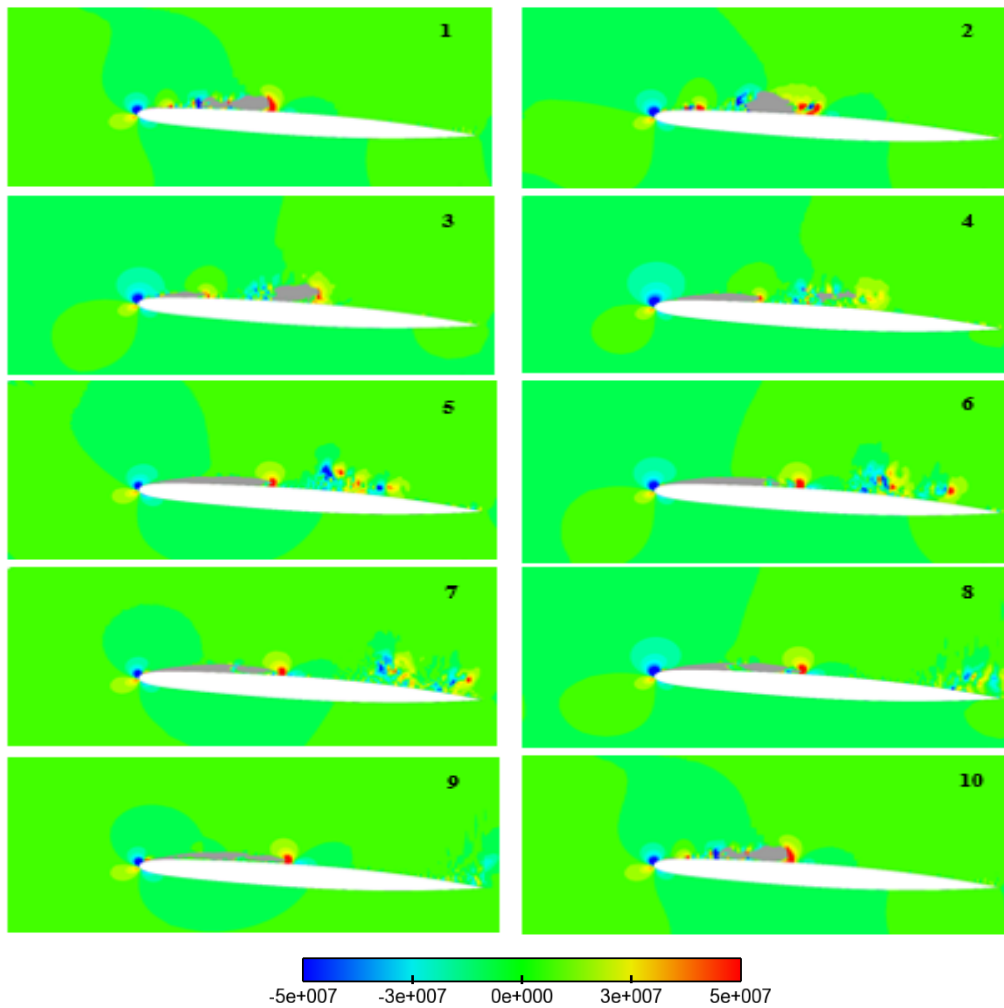


Fig. 8. Time evolution pressure gradient on x direction [$\text{kg m}^{-2} \text{s}^{-2}$] and the cavitation shedding for one cycle.

upstream along the surface of hydrofoil. It causes the rupture of the interface between the vapor pocket and the hydrofoil. It split and fragment the main cavity vapor into a small sheet (from time 6 to 8).

In time 9 and 10, a maximum pressure gradient just after the collapse at the leading edge of the hydrofoil is observed. After the detachment of the cavity vapor, the leading edge of the hydrofoil is free of vapor and a new vapor sheet starts to grow.

To identify numerically the influence of the pressure fluctuation due the cavitation shedding, we have placed five tap pressure at $x/c=0.1$; $x/c=0.3$, $x/c=0.5$; $x/c=0.7$ and $x/c=0.9$ from the leading edge on the suction surface (see Fig.9).

In Fig; 10, for the position $x/c=0.1$ the fluctuation of the pressure reach 5 bar during the collapse of the vapor cavity. For the position $x/c=0.3$ to $x/c=0.7$, we observe the progressive evolution of the amplitude pressure, this can be explained by the fact the development of the re-entrant jet which cause this signals.

The attenuation of the pressure fluctuation is

remarkable from the leading edge to the trailing edge of the hydrofoil. It is evident that for the position $x/c = 0.7$ is the closed region of the main cavity. Cons by, for $x/c= 0.9$, the pressure fluctuations is reduced substantially, this is due to the attachment of the flow on the surface of the hydrofoil.

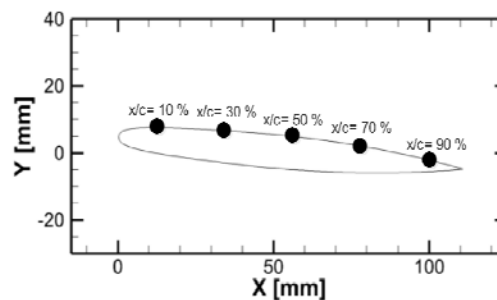


Fig. 9. Localization of the point tap.

We present in Fig. 11 the variation of the lift and

drag coefficients and the volume of vapor for one cycle only.

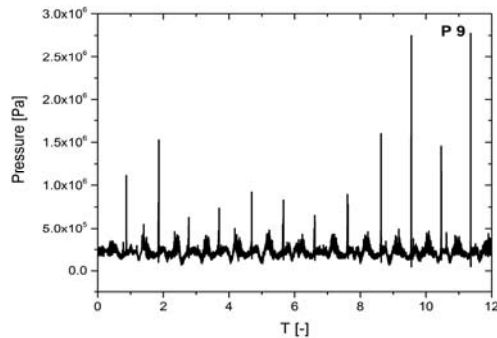


Fig. 10. Evolution of the pressure on extrados of the hydrofoil.

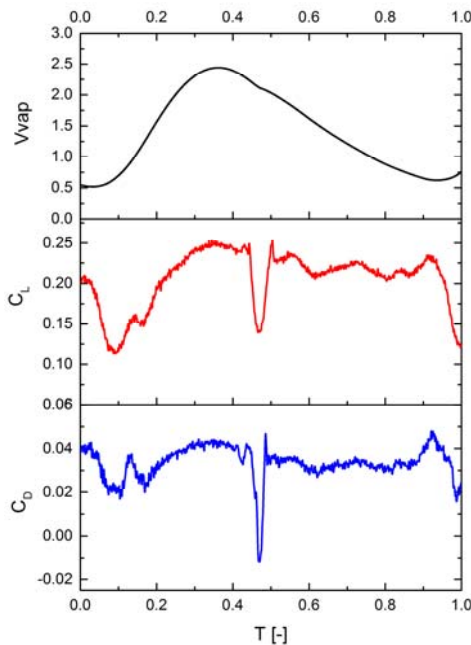


Fig. 11. Impact of developments of the vapor pocket on the drag and lift coefficient.

Referring to Fig.11, we note that the lift coefficient increases in parallel with the development of the vapor pocket on the upper surface of the hydrofoil. As the vapor pocket reaches the half the chord. The pressure within this pocket is equal to the saturation vapor pressure p_v , this causes an acting pressure gradient in Y axe, causing the increase in lift force.

In order to analyze the effect of the cavitation pocket on the separation of the flow, we present in fig. 12 two flow configurations (at the top without cavitation and at the bottom with cavitation). It is clear that the presence of the vapor pocket causes the separation of the flow. The attachment of the flow is localized in the closure region which is highly irregular and unsteady.

This process can be explained by the fact that the cavitation pocket accelerates the transition of the

laminar boundary layer to the turbulent boundary layer. On the other hand, if the same flow conditions are adopted without the presence of cavitation, it is emphasized that the boundary layer remains laminar until it reaches the trailing edge. Thus, the flow will remain attached to the wall of the hydrofoil.

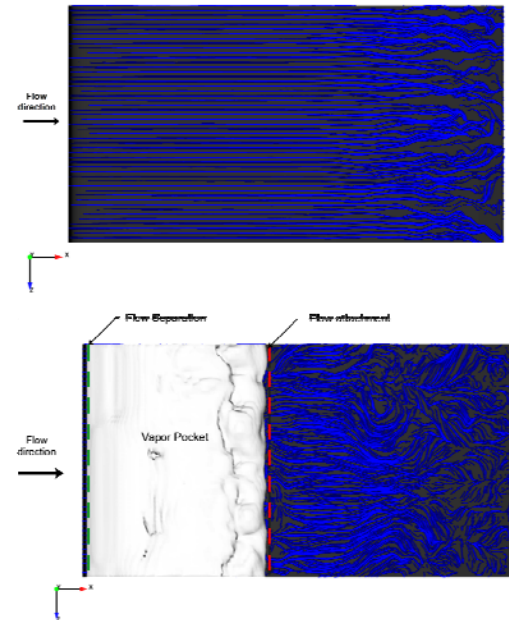


Fig. 12. Separation, attachment of the flow and the streamline (in blue color) over the hydrofoil, at the top without cavitation and at the bottom with cavitation.

Vortex shells produced by the cavitation shedding can be visualized as a positive isosurface of Q-criterion. This isosurface with positive Q isolates areas where the strength of the rotation overcomes the strain, thus making those surfaces eligible as vortex envelopes. The expression of the Q is defined as :

$$Q = \frac{1}{2}(\Omega_{ij}\Omega_{ij} - S_{ij}S_{ij}) \quad (16)$$

where

$$\Omega_{ij} = (u_{ij} - u_{ji})/2 \text{ and } S_{ij} = (u_{ij} + u_{ji})/2.$$

A positive value means the strength of the local rotations overcomes the local strain. Although the parameter used in the Q-criterion is still essentially the vorticity, this treatment of the Q-criterion eliminates the effect of the vorticity resulting from the boundary-layer flow where the local strain predominates.

The formation and development of the attached cavity and the shedding and collapse of the cavitation cloud can both be captured the iso-surfaces of both the Q-criterion and the vapor volume fraction.

However, a much more complex 3D structure can be obtained using the iso-surface of the Q-criterion

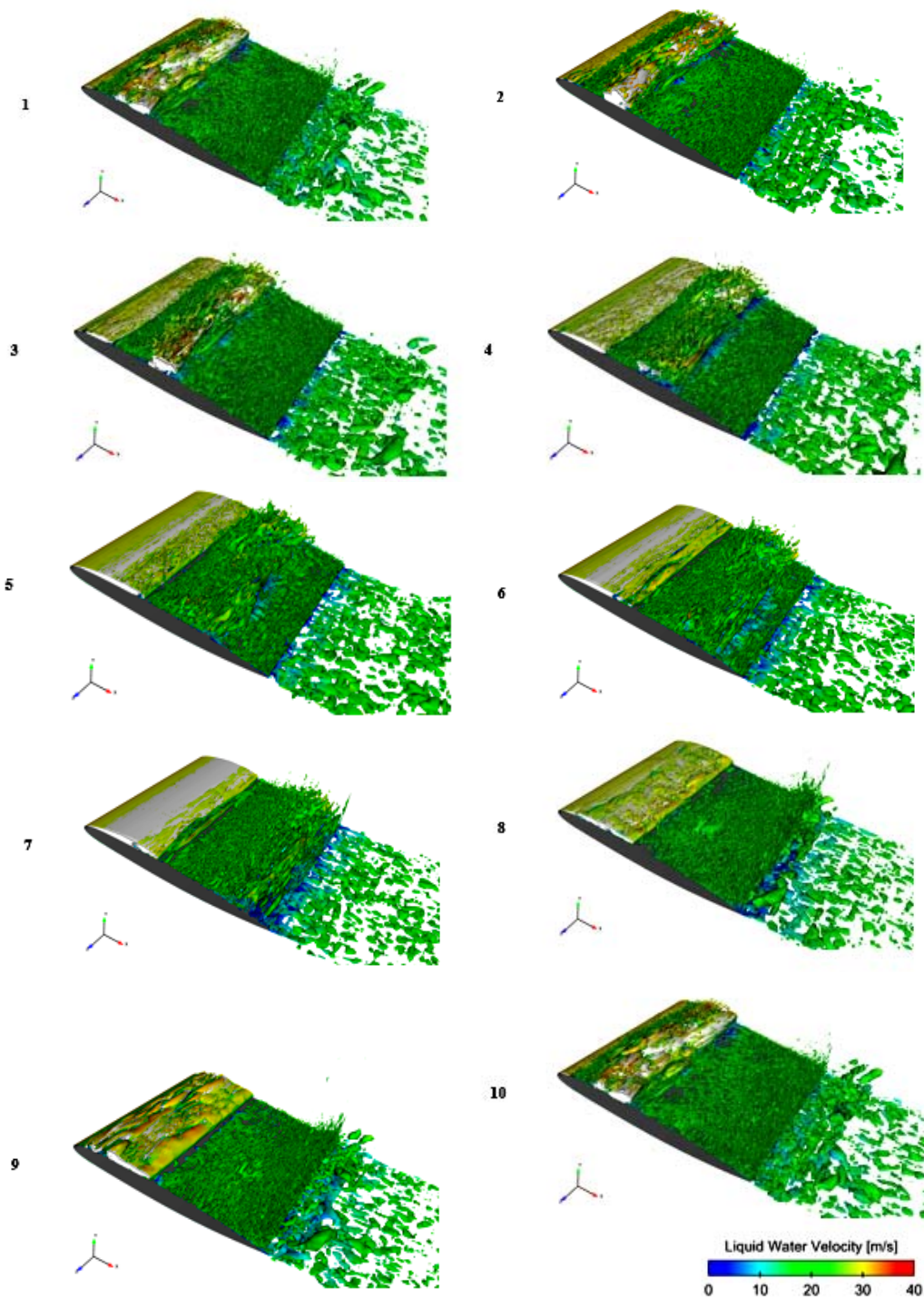


Fig. 13. Interaction of the flow structure and cavitating shedding.

than from the vapor volume fraction. Since the cloud cavity shedding is quite complex, the Q-criterion more accurately reflects the structure of the cavitation pattern. Since the Q-criterion accurately represents the relative magnitudes of the local rotation and the local strain or the vorticity distribution, the Q-criterion indicates a close connection between the vorticity and the cavitation.

Figure13, shows the evolution of the cavity shedding cycle and her impact on the structure of

the flow, colored according to the liquid velocity.

The vortex stretching mainly occurs in the center of the cloud cavity and changes quasi-periodically as the cloud cavity evolves. Not only is the distribution of the vortex stretching term strongly dependent on the cavity evolution, but also its magnitude.

Referring to Fig.13-1 to 13-4, the previously shed cavity cloud has caused the production of a high magnitude of the vortex stretching term vorticity in

the middle of the chord, the iso-surface of the criterion visualize the onset of the large flow structure with a high turbulence ratio. In this phase, the transfer and the destruction of the large structure to into a small structure Recognized as the energy cascade. The manifestation of the vorticity is well illustrated in Fig.13-5 and 13-6.

The magnitude of the vortex stretching close to its minimum and the vortex stretching is mainly near the rear of the foil. However, the distribution is quite different at where the vortex stretching covers nearly all of the suction side and at the same time the attached cavity is cut off near the leading edge by the re-entrant jet that induces the dramatic shedding of the cavitation cloud (from Fig.13-7 to13-10).

The numerical results indicate that the cloud cavitation is responsible for the production of the vortex stretching term.

Overall, the present simulation clearly reproduces the cavitation patterns and their evolution around the NACA0009 hydrofoil and captures the behaviors of the re-entrant flow well and shows a good agreement with experimental.

5. CONCLUSION

The unsteady cavitating flow around a NACA0009 hydrofoil was investigated numerically using LES coupled with the Kanfoudi cavitation model.

The mechanisms dictating the complex flow behaviors and the cavitation shedding dynamic evolution with the cavitation-vortex interaction were examined and summarized.

The vortex structure around the cavitating hydrofoil has been analyzed using Q-criterion variable.

The numerical results indicate that the cloud cavitation is responsible for the production of the vortex stretching term. The numerical results of the cavitating flow features are well reproduced by the numerical model and the main conclusions are:

1. The LES detected and resolved the flow structures which is responsible of the production of the pressure positive gradient which induces the re-entrant jet.
2. The dynamics of sheet cavitation generate strong pressure pulses due to the collapse of shed vapor structures. Within experiments, it is a difficult task to visualize these pressure pulses and the associated unsteady loading of the hydrofoil. In the present numerical results for cavitating flows these pressure pulses are predicted in detail.
3. The numerical model accurately predicts the formation of cavitation, with characteristic behavior, such as the cyclic formation of a sheet cavity, the formation of the re-entrant jet and the shedding of a vapor cloud;
4. the numerical results confirm the ability of the present model to predict the unsteady loading

of the hydrofoil due to the dynamics of the cavitating flow and due to the collapse of shed vapor structures;

5. Further analysis of the flow structure demonstrates that there is strong vortex-cavitation interaction with the shedding vapor cloud and the vortex stretching.

REFERENCES

- Altimira, M., L. Fuchs (2015). Numerical Investigation of Throttle Flow under Cavitating Conditions. *International Journal of Multiphase Flow* 75, 124–36.
- Amromin, E., J. Kopriva, E. A. Roger and M. Wosnik (2006). Hydrofoil Drag Reduction by Partial Cavitation. *Journal of Fluids Engineering* 128(5), 931.
- Arndt, R. (1981). Recent Advances in Cavitation Research. *ADV Hydrosoci* 12, 1–78.
- Arndt, R. E. A. (2001). Numerical Modeling of Sheet and Tip vortex Cavitation with Fluent 5 The Fluent 5 Cavitation Model. *Cavitation* (1972):1–8.
- Bensow, R. E., G. Bark (2010). Implicit LES Predictions of the Cavitating Flow on a Propeller. *J. Fluids Eng.* 132(4)1302.
- Callenaere, M., J. P. Franc, J. M. Michel and M. Riondet (2001). The Cavitation Instability Induced by the Development of a Re-Entrant Jet. *Journal of Fluid Mechanics* 444, 223–56.
- Chemloul, N. S. (2012). Experimental Study of Cavitation and Hydraulic Flip Effects on Liquid Jet Characteristics into Crossflows. *JAFM* 5(4), 33–43.
- Chen, G. H., G. Y. Wang, B. Huang, C. L. Hu, Z. Y. Wang and J. Wang (2015). Numerical Investigation of Dynamics of Unsteady Sheet/cloud Cavitating Flow Using a Compressible Fluid Model. *Modern Physics Letters B* 29.
- Chen, Y. and D. D. Heister (1994). A Numerical Treatment of Attached Cavitation. *Journal of Fluids Engineering* 116, 613–618.
- Davidson, L. and S. H. Peng (2003). Hybrid LES-RANS Modelling: A One-Equation SGS Model Combined with a K Model for Predicting Recirculating Flows. *International Journal for Numerical Methods in Fluids* 43(9), 1003–18.
- Deshpande, M., J. Feng and C. Merkle (1998). Numerical Modeling of the Thermodynamic Effects of Cavitation. *Journal of Fluids Engineering* 119, 420–427.
- Dieval, L., M. Arnoud and R. Marcer (1998). Numerical Modeling of Unsteady Cavitating Flows by a VoF Method. *Third International Symposium on Cavitation*.
- Dittakavi, N., A. Chunekar and S. Frankel (2010).

- Large Eddy Simulation of Turbulent-Cavitation Interactions in a Venturi Nozzle. *Journal of Fluids Engineering* 132(12), 121301.
- Dreyer, M., Decaix, J., Münch-Alligné, C., Farhat, M. 2014. Mind the Gap: A New Insight into the Tip Leakage Vortex Using Stereo-PIV. *Experiments in Fluids* 55:18–49.
- Foeth, E. J., C. W. H. Van Doorne, T. Van Terwisga and B. Wieneke (2006). Time Resolved PIV and Flow Visualization of 3D Sheet Cavitation. *Experiments in Fluids* 40(4), 503–13.
- Fujikawa, S. and T. Akamatsu (1980). Effects of the Non-Equilibrium Condensation of Vapour on the Pressure Wave Produced by the Collapse of a Bubble in a Liquid. *Journal of Fluid Mechanics* 79, 481–512.
- Goncalves, E., J. Decaix and R. F. Patella (2010). Unsteady Simulation of Cavitating Flows in Venturi. *Journal of Hydrodynamics* 22, 711–16
- Goncalvès, E.; Charrière, B. 2014. Modelling for Isothermal Cavitation with a Four-Equation Model. *International Journal of Multiphase Flow* 95:54–72.
- Gopalan, S. and J. Katz (2000). Flow Structure and Modeling Issues in the Closure Region of Attached Cavitation. *Physics of Fluids* 12, 895.
- Hirschi, R. and P. Dupont, F. Avellan, J. N. Favre, J. F. Guelich and E. Parkinson (1998). Centrifugal Pump Performance Drop due to Leading Edge Cavitation: Numerical Predictions Compared with Model Tests. *Journal of Fluids Engineering* 120, 705–711.
- Huang, B., G. y. Wang and Y. Zhao (2014). Numerical Simulation Unsteady Cloud Cavitating Flow with a Filter-Based Density Correction Model. *Journal of Hydrodynamics* 26(1), 26–36.
- Hutton, R. A. and S. P. Furness (1975). Experimental and Theoretical Studies of Two-Dimensional Fixed-Type Cavities. *ASME Transactions Journal of Fluids Engineering* 97, 515–521.
- ITTC. (1999). ITTC – Recommended Procedures ITTC – Recommended Procedures. *ReVision* 266–73.
- Jafarian, A., A. R. Pishavar (2016). Numerical Simulation of Steady Supercavitating Flows. *JAFM* 9(8), 2981–92.
- Ji, B. and *et al.* (2014). Large Eddy Simulation and Theoretical Investigations of the Transient Cavitating Vortical Flow Structure around a NACA66 Hydrofoil.
- Ji, B., X. Luo, Y. Wu, X. Peng and Y. Duan (2013). Numerical Analysis of Unsteady Cavitating Turbulent Flow and Shedding Horse-Shoe Vortex Structure around a Twisted Hydrofoil. *International Journal of Multiphase Flow* 51, 33–43.
- Kanfoudi, H. (2011). A Numerical Model to Simulate the Cavitating Flows. *International Journal of Modeling, Simulation, and Scientific Computing* 2(3), 277–97.
- Kanfoudi, H. (2012). Numerical Investigation for Steady and Unsteady Cavitating Flows. in *INTECH*.
- Kanfoudi, H. (2014). Modelling of Unsteady Cavitating Flow Hatem Kanfoudi , Hedi Lamoumi and Ridha Zgolli. *International Journal of Renewable Energy Technology* 5(2), 20–22.
- Kanfoudi, H. (2015). Modeling and Computation of the Cavitating Flow in Injection Nozzle Holes. *International Journal of Modeling, Simulation, and Scientific Computing* 6(1), 1550003.
- Katz, J. (1986). Cavitation in Large Scale Shear Flows. *Journal of Fluids Engineering* 108, 373–76.
- Katz, J. and T. O’Hern (1986). Cavitation in Large Scale Shear Flows. *Journal of Fluids Engineering* 108, 373–76.
- Koo, Heeseok, P. Donde and V. Raman (2013). LES-Based Eulerian PDF Approach for the Simulation of Scramjet Combustors. *Proceedings of the Combustion Institute* 34(2), 2093–2100.
- Koop, A. H. (2008). Numerical Simulation of Unsteady Three-Dimensional Sheet Cavitation.
- Kozubková, M., J. Rautová and M. Bojko (2012). Mathematical Model of Cavitation and Modelling of Fluid Flow in Cone. *Procedia Engineering* 39, 9–18
- Kravtsova, A. Y., D. M. Markovich, K. S. Pervunin, M. V. Timoshevskiy and K. Hanjalić (2014). High-Speed Visualization and PIV Measurements of Cavitating Flows around a Semi-Circular Leading-Edge Flat Plate and NACA0015 Hydrofoil. *International Journal of Multiphase Flow* 60, 119–34.
- Kubota, A.; H. Kato and H. Yamaguchi (1992). A New Modelling of Cavitating Flows; A Numerical Study of Unsteady Cavitation on a Hydrofoil Section. *Journal of Fluid Mechanics* 240, 59–96.
- Kuijpers, M. W. A., D. V. Eck, M. F. Kemmere and J. T. F. Keurentjes (2002). Cavitation-Induced Reactions in High-Pressure Carbon Dioxide. *Science (New York, N. Y.)* 298, 1969–71.
- Kunz, R. F., T. Kaday, J. W. Lindau and L. J. Peltier (2003). Unsteady Rans and Detached Eddy Simulations of. *Fifth International Symposium on Cavitation (CAV2003)* 1–12.

- Lee, T. S., H. T. Low and D. Nguyen (2008). Effects of Air Entrainment on Fluid Transients in Pumping Systems. *JAFM* 1(1), 55–61.
- Luo, X. W., B. Ji and Y. Tsujimoto (2016). A Review of Cavitation in Hydraulic Machinery. *Journal of Hydrodynamics, Ser. B* 28, 335–58.
- Martynov, S. (2005). Numerical Simulation of the Cavitation Process in Diesel Fuel Injectors. *Analysis* 1–226.
- Menter, F. R. (1994). Two-Equation Eddy-Viscosity Turbulence Models for Engineering Applications. *AIAA Journal* 32(8), 1598–1605.
- Molin, B., L. Dieval, R. Marcer and M. Arnaud (1997). Non-Stationary Model for Cavitating Sheet by the Use of a Potential Method and a VoF Method. *6th Journées des l’Hydromécanique* 31–44.
- Moussatov, A., C. Granger and B. Dubus (2005). Ultrasonic Cavitation in Thin Liquid Layers. *Ultrasonics Sonochemistry* 12(6), 415–22.
- Nur, M., M. M. Karim, M. d. Manirul and A. Sarker (2016). Numerical Prediction of Unsteady Behavior of Cavitating Flow on Hydrofoils Using Bubble Dynamics Cavitation Model. *JAFM* 9(6), 1829–37.
- O’Brien, W. D. *et al.* (2000). Ultrasound-Induced Lung Hemorrhage Is Not Caused by Inertial Cavitation. *The Journal of the Acoustical Society of America* 108(3), 1290–97.
- Oprea, A. and N. Bulten (2011). Cavitation Modelling Using RANS Approach. *WIMRC 3rd Int. Cavitation Forum* 2,1–10.
- Pankaj, G., R. Saini (2016). Numerical Study of Cavitation in Francis Turbine of a Small Hydro Power Plant. *JAFM* 9(1), 357–65.
- Payri, F., R. Payri, F. J. Salvador and J. Martínez-Lpez (2012). A Contribution to the Understanding of Cavitation Effects in Diesel Injector Nozzles through a Combined Experimental and Computational Investigation. *Computers and Fluids* 58, 88–101.
- Pendar, M. R. and E. Roohi (2016). Investigation of Cavitation around 3D Hemispherical Head-Form Body and Conical Cavitators Using Different Turbulence and Cavitation Models. *Ocean Engineering* 112, 287–306.
- Peng, X. X.; B. Ji, Y. Cao, L. Xu, G. Zhang, X. Luo and X. Long (2016). Combined Experimental Observation and Numerical Simulation of the Cloud Cavitation with U-Type Flow Structures on Hydrofoils. *International Journal of Multiphase Flow* 79, 10–22.
- Pope, S. B. (2000). *Turbulent Flows*.
- Rayleigh, L. (1917). On the Pressure Developed in a Liquid during the Collapse of a Spherical Cavity. *Philosophy Magazine* 3, 94–98.
- Roohi, E., A. P. Zahiri and M. Passandideh Fard (2013). Numerical Simulation of Cavitation around a Two-Dimensional Hydrofoil Using VOF Method and LES Turbulence Model. *Applied Mathematical Modelling* 37(9), 6469–88.
- Roohi, E., A. P. Zahiri, M. Passandideh Fard (2013). Numerical Simulation of Cavitation around a Two-Dimensional Hydrofoil Using VOF Method and LES Turbulence Model. *Applied Mathematical Modelling* 37, 6469–88.
- Sagaut, P. (2005). Large Eddy Simulation for Incompressible Flows: An Introduction (Scientific Computation): P. Sagaut, Charles Meneveau: 9783540263449: Amazon.com: Books. *Springer* 558.
- Salleo, S., A. Nardini, F. Pitt and M. A. Lo Gullo (2000). Xylem Cavitation and Hydraulic Control of Stomatal Conductance in Laurel (*Laurus Nobilis* L.). *Plant, Cell and Environment* 23(1), 71–79.
- Santosh, M., S. Shatendra, A. Choudhury (2014). CFD Investigation of Influences of Reverse Textures on Bearing Surface of a Journal Bearing. *JAFM* 7, 395–99.
- Sauer, J. (2000). Instationar Kavitierende Stromungen - Ein Neues Modell, Basierend Auf Front Capturing (VoF) Und Blasendynamik. Karlsruhe University.
- Schnerr, G. H., I. H. Sezal and S. J. Schmidt (2008). Numerical Investigation of Three-Dimensional Cloud Cavitation with Special Emphasis on Collapse Induced Shock Dynamics. in *Physics of Fluids* 20.
- Senocak, I. and W. Shyy (2004). Interfacial Dynamics Based Modelling of Turbulent Cavitating Flows, Part 1: Model Development and Steady State Computations. *International Journal for Numerical Methods in Fluids* 995(October 2003), 975–95.
- Shia Hui, P. and H. Werner (2008). *Advances in Hybrid RANS-LES Modelling*.
- Shur, M. L., P. R. Spalart, M. K. Strelets and A. K. Travin (2008). A Hybrid RANS-LES Approach with Delayed-DES and Wall-Modelled LES Capabilities. *International Journal of Heat and Fluid Flow* 29(6), 1638–49.
- Singhal, A. K., M. M. Athavale, H. Li and Y. Jiang (2002). Mathematical Basis and Validation of the Full Cavitation Model. *Journal of Fluids Engineering* 124(3), 617.
- Smagorinsky, J. (1963). General Circulation Experiments with the Primitive Equations I: The Basic Experiment. *Monthly Weather Review*, 91–99.

- Stutz, B. and J. L. Reboud (1997). Experiments on Unsteady Cavitation. *Experiments in Fluids* 22(3), 191–98.
- Stutz, B. and J. L. Reboud (1997). Two-Phase Flow Structure of Sheet Cavitation. *Physics of Fluids* 9(12), 3678.
- Suh, H. K. and C. S. Lee (2008). Effect of Cavitation in Nozzle Orifice on the Diesel Fuel Atomization Characteristics. *International Journal of Heat and Fluid Flow* 29(4), 1001–9.
- Timoshevskiy, M. V., S. A. Churkin, A. Y. Kravtsova, K. S. Pervunin, D. M. Markovich, K. Hanjalić (2016). Cavitating Flow around a Scaled-down Model of Guide Vanes of a High-Pressure Turbine. *International Journal of Multiphase Flow* 78, 75–87.
- Walters, D. K., S. Bhushan, M. F. Alam and D. S. Thompson (2013). Investigation of a Dynamic Hybrid RANS/LES Modelling Methodology for Finite-Volume CFD Simulations. *Flow, Turbulence and Combustion* 91 643–67.
- Wang, G., I. Senocak, W. Shyy, T. Ikohagi and S. Cao (2001). Dynamics of Attached Turbulent Cavitating Flows. *Progress In Aerospace Sciences* 37, 551–81.
- Wang, T. Y., K. Y. Lai, C. Y. Lai and P. C. Li (2005). A Study on Microbubble-Assisted Acoustic Cavitation. *Journal of Medical and Biological Engineering* 25(4), 165–70.
- Wang, X. and W. Su (2010). Numerical Investigation on Relationship between Injection Pressure Fluctuations and Unsteady Cavitation Processes inside High-Pressure Diesel Nozzle Holes. *Fuel* 89(9), 2252–59.
- Wilcox, D. C. (1988). Reassessment of the Scale-Determining Equation for Advanced Turbulence Models. *AIAA Journal* 26(11), 1299–1310.
- Wilcox, D. C. (1994). Simulation of Transition with a Two-Equation Turbulence Model. *AIAA Journal* 32(2), 247–55.
- Wosnik, M., R. Arndt and Q. Ain (2006). Identification of Large Scale Structures in the Wake of Cavitating Hydrofoils Using LES and Time-Resolved PIV. in *Proc. 26th Symposium on Naval Hydrodynamics*. Roma.
- Wu, J., G. Wang and W. Shyy (2005). Time-Dependent Turbulent Cavitating Flow Computations with Interfacial Transport and Filter-Based Models. *International Journal for Numerical Methods in Fluids* 49(7), 739–61.
- Wu, X. C., Y. W. Wang and C. G. Huang (2016). Effect of Mesh Resolution on Large Eddy Simulation of Cloud Cavitating Flow around a Three Dimensional Twisted Hydrofoil. *European Journal of Mechanics - B/Fluids* 55, 229–40.
- Y. AitBouziad (2005). Physical Modelling of Leading Edge Cavitation: Computational Methodologies and Application To Hydraulic Machinery. *Thèse de IEPFL* 3353.
- Yan, Y. and R. B. Thorpe (1990). Flow Regime Transitions due to Cavitation in the Flow through an Orifice. *International Journal of Multiphase Flow* 16(6), 1023–45.
- Yu, X., C. Huang, T. Du, L. Liao, X. Wu, Z. Zheng, Y. Wang (2014). Study of Characteristics of Cloud Cavity Around Axisymmetric Projectile by Large Eddy Simulation. *Journal of Fluids Engineering* 136.
- Yuan, W., J. Sauer and G. H. Schnerr (2001). Modeling and Computation of Unsteady Cavitation Flows in Injection Nozzles. *Mec. Ind* 2, 383–394.
- Yuan, W., J. Sauer and G. H. Schnerr (2001). Modeling and Computation of Unsteady Cavitation Flows in Injection Nozzles. *Mecanique et Industries* 2(5), 383–94.
- Zhang, L. X. and B. C. Khoo (2013). Computations of Partial and Super Cavitating Flows Using Implicit Pressure-Based Algorithm (IPA). *Computers and Fluids* 73, 1–9.
- Zhao, Y., G. Wang and B. Huang (2016b). A Curvature Correction Turbulent Model for Computations of Cloud Cavitating Flows. *Engineering Computations* 33(1), 202–16. Retrieved.
- Zhao, Yu, G. Wang and B. Huang (2016a). A Curvature Correction Turbulent Model for Computations of Cloud Cavitating Flows. *Engineering Computations* 33(1), 202–16. Retrieved September 30.
- Zhu, J., Y. Chen, D. Zhao and X. Zhang (2015). Extension of the Schnerr-Sauer Model for Cryogenic Cavitation. *European Journal of Mechanics, B/Fluids* 52, 1–10.
- Zwart, P. J., A. G. Gerber and T. Belamri (2004). A Two-Phase Flow Model for Predicting Cavitation Dynamics. in *ICMF 2004 International Conference on Multiphase Flow*.